Corrosion behavior of Fe-Cr-Al alloys with yttrium addition on 360 ℃ simulated pressurized water chemistry condition

Taeyong Kim[a], Sungyu Kim[b], Seung Chang Yoo[a], Junhyuk Ham[a], Yunju Lee[a], Song In Young[a], Chi Bum Bahn[b] and Ji Hyun Kim [*a]
[a]*Department of Nuclear Engineering, College of Engineering*
Ulsan National Institute of Science and Technology, 50 UNIST-gil, Banyeon-li, Ulju-gun, Eonyang-eup, Ulsan, 44919
[b]*School of Mechanical Engineering, Pusan National University, 2 Busandaehak-ro, 63beon-gil, Geumjeong-gu, Busan 46241, Republic of Korea*
**Corresponding author: kimjh@unist.ac.kr*

1. Introduction

When pressurized water reactor occurs beyond designed based accident, Zr based alloys generate hydrogen gas by reacting with high temperature steam. Fe-Cr-Al alloy can mitigate the increment of cladding temperature and hydrogen generation at the severe accident condition. However, the chemical composition of Fe-Cr-Al alloy is not yet optimized. This research investigates corrosion behavior of Fe-Cr-Al alloys including various chemical elements at normal operation condition to evaluate whether it could be used as accident-tolerance fuel cladding.

Chromium and aluminum are the major elements contributing to the formation of protective oxide films. The amount of the two elements were decided carefully since too much Cr or Al can generate α'-Cr phase or worsen the workability. Also, yttrium can achieve slower growth rate and thicker oxide film. Based on these facts, we selected specimens of Fe14Cr4Al, Fe14Cr4Al-Y and Fe13Cr6Al-Y. Those specimens were immersed to simulated primary water environment for 83 days. And the corrosion resistance of three specimens was analyzed through Optical Microscope (OM), Scanning Electron Microscope (SEM), Energy Dispersive X-ray Spectroscopy (EDS), and X-Ray Diffraction (XRD).

2. Experimental

2.1 Alloys

The accident tolerant fuel cladding to be subjected to the long-term corrosion test was tested on the Fe13Cr6Al-Y alloy, which has a high oxidation resistance, in the Cr, Al and Y contents of the alloy composition calculated from the thermodynamic basis in the past study. The Fe14Cr4Al alloy and the Fe14Cr4Al-Y alloy were charged at the same time to compare the effects of Y content and Cr and Al contents.

2.2 Water chemistry condition

Temperature is one of the factors affecting the corrosion behavior of the cladding in the primary environment of a nuclear power plant. The temperature and pressure conditions on the primary side of the nuclear power plant are shown in Table 1-1, but the corrosion behavior of the cladding tube is crucial to the temperature of the cladding tube itself. Therefore, in this experiment, the temperature of the cooling water circulating inside the experimental apparatus was maintained at 360 °C to match the temperature of the actual cladding tube of 360 °C. Also, to prevent the boiling of the cooling water, the pressure inside the experimental apparatus was 20 MPa. During the corrosion of the cladding material, the elements inside the cladding material are eluted and bonded with the oxygen of the coolant. This phenomenon is influenced by the water chemistry environment of the coolant. Table 1-2 shows the water chemistry conditions applied to the primary environment of the nuclear power plant. In addition, as the corrosion experiment is prolonged, the elements in the cladding material can be eluted to change the quality of the cooling water. Therefore, the water chemistry environment of the experimental apparatus was maintained by circulating the cooling water at a flow rate of about 150 mL / min suitable for the high temperature and high-pressure corrosion test according to ASTM 111-97.

Table I: Chemical composition in wt. %

	Fe	Cr	Al	Y
Fe14Cr4Al	Bal.	13.5	3.4	-
Fe14Cr4Al-Y	Bal.	13.872	3.78	0.149
Fe13Cr6Al-Y	Bal.	12.526	5.501	0.143

Table II: Temperature and pressure for primary water and simulated system

for primary water system		for simulated system	
Pressure	Temperature	Pressure	Temperature
15.5 MPa	292-325 °C	20 MPa	360 °C

Table III: Water chemistry in simulated system

B(ppm)	Li(ppm)	DO(ppb)	pH
1000-1200	2	< 10	6.8-7.4

3. Results

3.1 Weight change

The weight of both as-received and corroded FeCrAl alloy specimens was measured three times. And weight change per unit area of that was calculated as dividing by all area of each sample. At Fig. 1, the results of weight change were almost negligible; ± 0.1 mg/cm^2 for every specimen. As a result, all three alloys show high corrosion resistance through three months corrosion test. As shown in Fig. 2, 3 and 4, Fe14Cr4Al alloy and Fe13Cr6Al-Y alloy showed larger weight loss and larger weight increase than Fe14Cr4Al-Y alloy. However, because the variation width is very small, relative comparisons of each other are not appropriate for comparing corrosion performance. As a result of less than 3 months compared to the reactor operation time, sufficient oxide film was not formed in the comparison, so it is required to perform the weight comparison through corrosion experiment for one year.

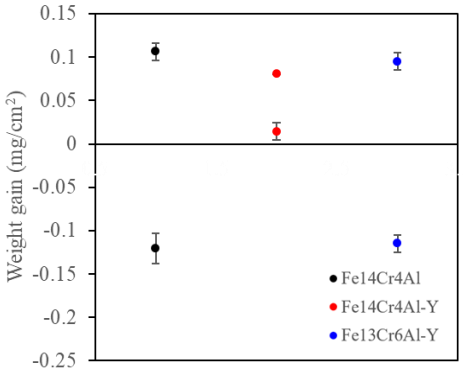

Fig. 1. Mass change of FeCrAl alloys exposed to the simulated primary environment water chemistry condition of nuclear power plant for 83 days

3.2 Optical Microscope (OM) analysis

From OM analysis, all specimens had oxide film, and Y-containing specimens included small white particles on the surface.

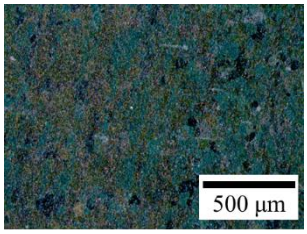

Fig. 2. OM analysis of Fe14Cr4Al alloy.

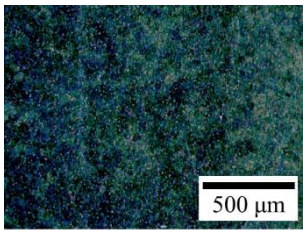

Fig. 3. OM analysis of Fe14Cr4Al-Y alloy.

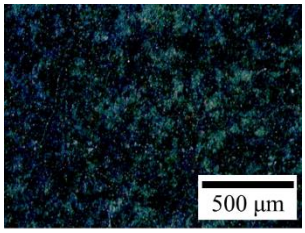

Fig. 4. OM analysis of Fe13Cr6Al-Y alloy.

3.3 Scanning Electron Microscope (SEM) analysis

Fe14Cr4Al specimen had 250-300 nm of oxide film, while Y-containing specimen had 200 nm of oxide film. There were Y oxide particles on the surface of the oxide film, and the size of those were about 0.5 μm to 1 μm. Moreover, oxide film was formed and extended around Y oxide. From the results of EDS, Fe and Cr elements composed surface of oxide film of all three specimens.

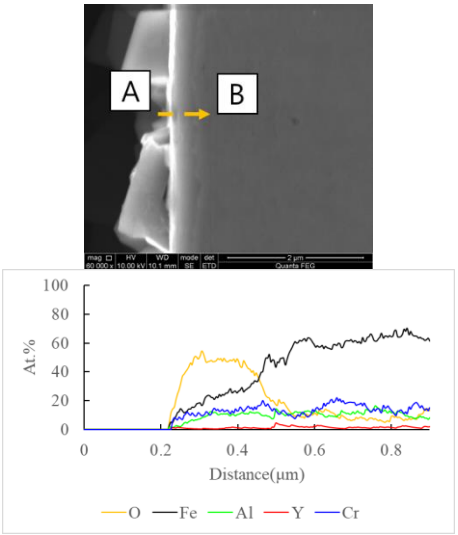

Fig. 5. Microstructure observation and composition analysis of Fe14Cr4Al alloy by SEM.

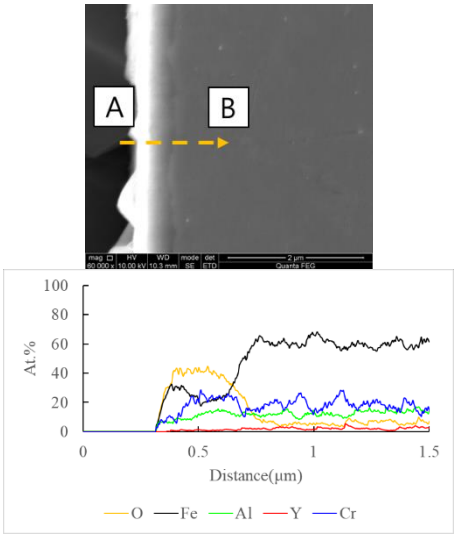

Fig. 6. Microstructure observation and composition analysis of Fe14Cr4Al-Y alloy by SEM.

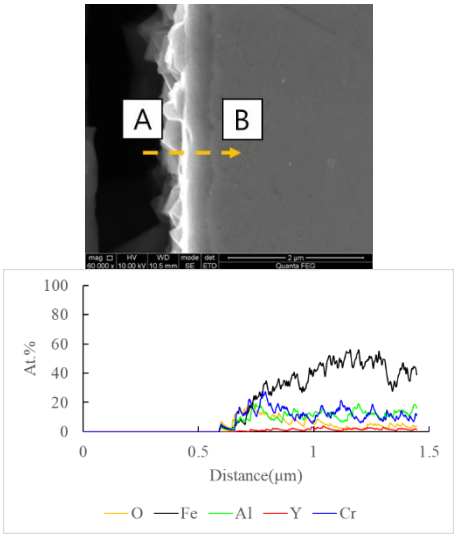

Fig. 7. Microstructure observation and composition analysis of Fe13Cr6Al-Y alloy by SEM.

3.4 Computational thermodynamics calculation

The microstructure and depth composition of the oxide film was confirmed by the analysis so far. However, in order to precisely analyze the structure of the oxide, it is predicted through computational thermodynamics calculation, and finally, the oxide film is identified through an X-ray diffractometer. Fig. 8, 9, 10 and 11 show the types of oxide films that can be produced in the FeCrAl-Y alloy exposed to the 360 ° C environment obtained through the HSC computational thermodynamics program. The Fe and Cr elements are likely to form $FeCr_2O_4$ oxides and the Al element will form AlO(OH) oxides. In the case of Y elements, they may form oxygen and form Y_2O_3. It can be confirmed that the above composition analysis and the corresponding oxide results agree with each other except AlO(OH).

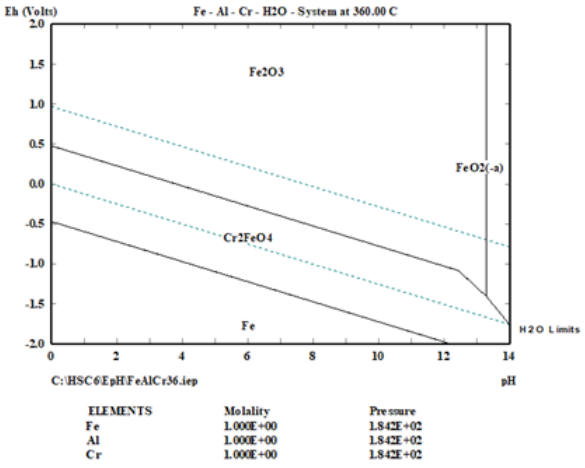

Fig. 8. Fe-related production phase derived from HSC computational thermodynamics.

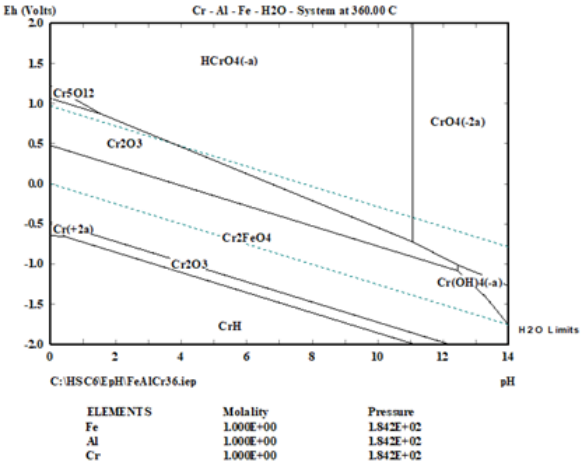

Fig. 9. Cr-related production phase derived from HSC computational thermodynamics.

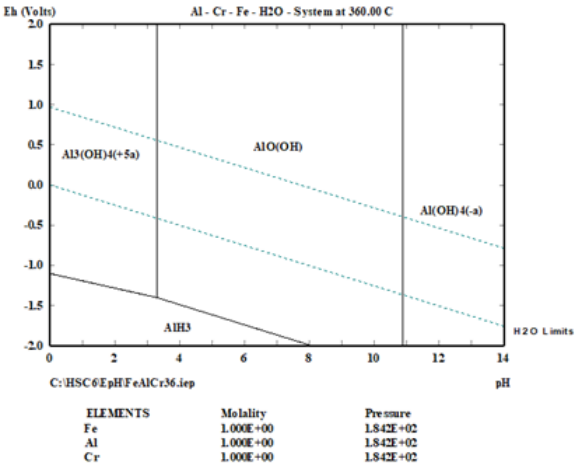

Fig. 10. Al-related production phase derived from HSC computational thermodynamics.

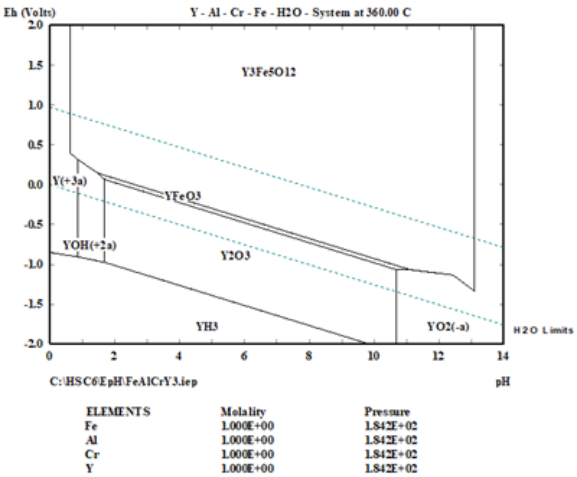

Fig. 11. Y-related production phase derived from HSC computational thermodynamics.

3.5 Identification of oxide film by high resolution X-ray diffractometer

Fig. 12 shows that the $FeCr_2O_4$ and Al_2O_3 oxide layers were formed by X-ray diffraction analysis of the FeCrAl corrosion specimens analyzed in this experiment through diffraction analysis. In the case of the Fe_2O_3 and Cr_2O_3 diffraction phases, it was confirmed that the diffraction image with the highest intensity could not be confirmed. In the case of Y_2O_3, the diffraction image can not be confirmed because a very small amount exists locally. In the Al_2O_3 diffraction phase, it is judged that the diffraction image agrees exactly, but it is too early to conclude that the diffraction image is generated because of the reason such as the deformation due to the force acting on the oxide film. Further analysis will be carried out to identify Al oxide.

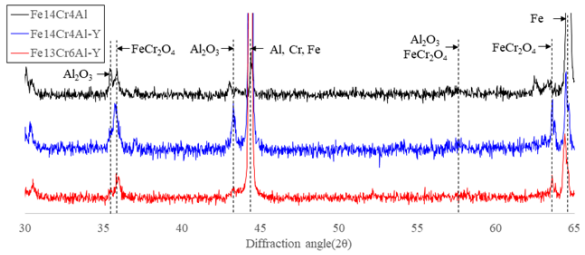

Fig. 12. Diffraction phase through HRXRD of FeCrAl alloy.

4. Conclusions

Fe14Cr4Al, Fe14Cr4Al-Y and Fe13Cr6Al-Y alloy specimens were exposed to the simulated primary water chemistry condition of nuclear power plant for 83 days. The weight change of that is negligible about 0.1 mg/cm2. However, Y addition alloys like Fe14Cr4Al-Y and Fe13Cr6Al-Y shows thin oxide scale about 200 nm which is smaller than the scale of Fe14Cr4Al without Y. From the HRXRD, the chemical composition of the scale formed on all alloy specimens is composed of $FeCr_2O_4$ and Al_2O_3. Intensity of Al_2O_3 phase is increased by adding the Y element. Then, the Al2O3 phase in oxide scale seem to increase the corrosion resistance. Although, the scale of Fe13Cr6Al specimens didn't show apparent Al_2O_3 phase peak, the high Al content might be influence on the enhanced corrosion resistance. Therefore, the addition of Y element can improve the long-term corrosion integrity of the cladding tube, and the mechanism of the corrosion resistant behavior of Y element will be studied in the future.

ACKNOWLEDGMENTS

This work was supported by the National Nuclear R&D programs (NRF-2019M2D1A1067205) organized by the National Research Foundation (NRF) of South Korea in support of the Ministry of Science and ICT (MSIT).

This work was financially supported by a Human Resources Development of the Korea Institute of Energy Technology Evaluation and Planning grant (No. 20194030202400) funded by the Korea Government Ministry of Trade Industry and Energy.

REFERENCES

[1] M. Short, R. G. Ballinger, A Functionally Graded Composite for Service in High-Temperature Lead-and Lead-Bismuth-Cooled Nuclear Reactors-1: Design, Nuclear Technology, Vol.177, p. 366-381, 2012.
[2] Z. Jiao, and G. S. Was, Segregation behavior in proton- and heavy-ion-irradiated ferritic-martensitic alloys, Acta Materialia, Vol.59, p. 4467-4481, 2011.
[3] M. P. Short, S. Morton, S. E. Ferry, and R. G. Ballinger, Diffusional stability of ferritic-martensitic steel composite for service in advanced lead-bismuth cooled nuclear reactors. International Heat Treatment and Surface Engineering, International Heat treatment and Surface engineering, vol.4, p. 74-80, 2013.
[4] J. F. Ziegler et al., SRIM-The Stopping and range of Ions in Solids. 2009
[5] H.H. Shen et al., proton irradiation effects on the precipitate in a Zr-1.6Sn-0.6Nb-0.2Fe-0.1Cr alloy, Journal of Nuclear Materials, Vol.452, p. 335-342, 2014
[6] Friedrich Garzarolli et al., effect of high neutron fluences on microstructure and growth of zircaloy-4, ASTM, 1989.